Mass Segregation in Eccentric Nuclear Disks: Enhanced Tidal Disruption Event Rates for High Mass Stars

by

Hayden R. Foote

Bachelor of Arts – Department of Astrophysical & Planetary Sciences

Undergraduate Honors Thesis

Thesis Defense Committee:

Prof. Ann-Marie Madigan	Thesis Advisor	Department of APS
Prof. Erica Ellingson	Honors Council Representative	Department of APS
Prof. Scot Douglass	External Faculty Member	Herbst Program of Humanities

Defended on:

April 2, 2020

Draft version April 17, 2020
Typeset using LaTeX **preprint** style in AASTeX62

ABSTRACT

Eccentric nuclear disks are a type of star cluster found in galaxy nuclei in which the stars lie on highly elliptical, spatially–aligned orbits in a disk around the central supermassive black hole. The closest such disk lies in our nearest large neighbor galaxy, Andromeda. Gravitational interactions between stars stabilize these disks, and can also send stars perilously close to the central black hole. If a star gets close enough, the black hole's extreme gravity will tear the star apart in a tidal disruption event. These tidal disruption events are observable with Earth–based telescopes, and are of rising interest to astronomers studying high–energy events. Computer simulations of eccentric nuclear disks are a useful tool to constrain how often we might expect to see a tidal disruption event from a galaxy that harbors an eccentric nuclear disk. In an effort to make these simulations more realistic, we conduct the first study of eccentric nuclear disks that considers stars of different masses. We show that more massive stars tend to be found at the inner edge of the disk, on orbits that lie close to the disk's midplane. These two effects make heavy stars more susceptible to tidal disruption, which manifests as a factor of 2-3 increase in the fraction of heavy stars that disrupt vs. light stars.

Contents

1. INTRODUCTION

Every large galaxy harbors a supermassive black hole with a mass ranging from one million to over ten billion times the mass of our Sun. These monster black holes lie at the very centers of their host galaxies, and each is immediately surrounded by a cluster of stars that orbit the black hole under the influence of its gravity.

Most of these star clusters, including the one at the center of our Milky Way, are spherical in shape with stars on elliptical orbits that collectively form a roughly ball-shaped cluster. However, at the center of our nearest large neighbor, the Andromeda Galaxy (M31), lies a very different arrangement of stars. *Hubble Space Telescope* (HST) images of the nucleus of M31 show two bright clusters of stars, both offset from the supermassive black hole (Lauer et al. 1993).

Tremaine (1995) explained this curious image, positing that the two bright clusters in the image are actually a single collection of stars orbiting the black hole. The stars at the center of M31 lie in an Eccentric Nuclear Disk (END), a thin disk of stars on elliptical orbits, where the orbits are oriented in the same direction in space. The two bright spots on the Hubble image correspond to the points of furthest and closest approach to the black hole of the disk stars.

Recently, Madigan et al. (2018) used simulations of ENDs to demonstrate that they are dynamically stable, that is, they will retain their basic structure over long periods of time. Additionally, they showed that ENDs throw stars towards the central black hole at very high rates. When a star passes too close to the black hole, tidal gravity from the black hole overcomes the star's self–gravity and tears the star apart in a Tidal Disruption Event (TDE) (Rees 1988). These TDEs are comparable in brightness to supernovae, and several have been observed as bright flares from the centers of their host galaxies (van Velzen et al. 2011; Gezari et al. 2012; Arcavi et al. 2014; Chornock et al. 2014; Holoien et al. 2016; Auchettl et al. 2017). The tendency of ENDs to produce many TDEs makes them highly interesting structures to study.

Initial simulations by Madigan et al. (2018) were effective at revealing the basic dynamics of an END, but they were far from realistic. In particular, all of the stars in their simulations had the same mass. In reality, the stars in any cluster have a wide spectrum of masses, and because the stars in a cluster feel gravity from each other as well as the central black hole, stars of different mass behave differently. In this work, we conduct simulations including two different populations of stars with different masses. This will trigger a dynamical mechanism called mass segregation, whereby the more massive stars in the disk will sink to its inner edge, while the less massive stars move towards the outer edge. We expect that this mass segregation will affect the TDE rates from ENDs, and so aim to quantify this effect.

This work is organized as follows: In § 2, we provide necessary background information, including how orbits are described, relevant dynamical processes, and more in-depth discussions of TDEs and ENDs. In § 3, we present our methods, including setup and initial conditions of our simulations. In § 4, we show the results of our simulations, including radial mass segregation, vertical mass segregation, and how these affect TDE rates from ENDs. In § 5, we discuss how this work may be applied to real systems, and a few implications of our results. In § 6, we summarize our findings.

2. BACKGROUND

2.1. *Orbits and The Kepler Elements*

Here, we discuss the orbit of a body around a central object, and various parameters that are used to describe the orbit and the motion of the body.

In three-dimensional space, fully determining the motion of an object requires six numbers. In orbital mechanics these six numbers are the Kepler elements, which together completely describe the orbit of a body around a central object, as well as where the body is on that orbit. A visual representation of the Kepler elements is shown in Figure 1.

Kepler's first law of orbital motion states that orbits are ellipses, with the central object at one focus of the ellipse. The first two orbital elements, semimajor axis and eccentricity, describe that ellipse. *Semimajor axis* (a) is a distance describing how large the orbit is, and is equal to half of the

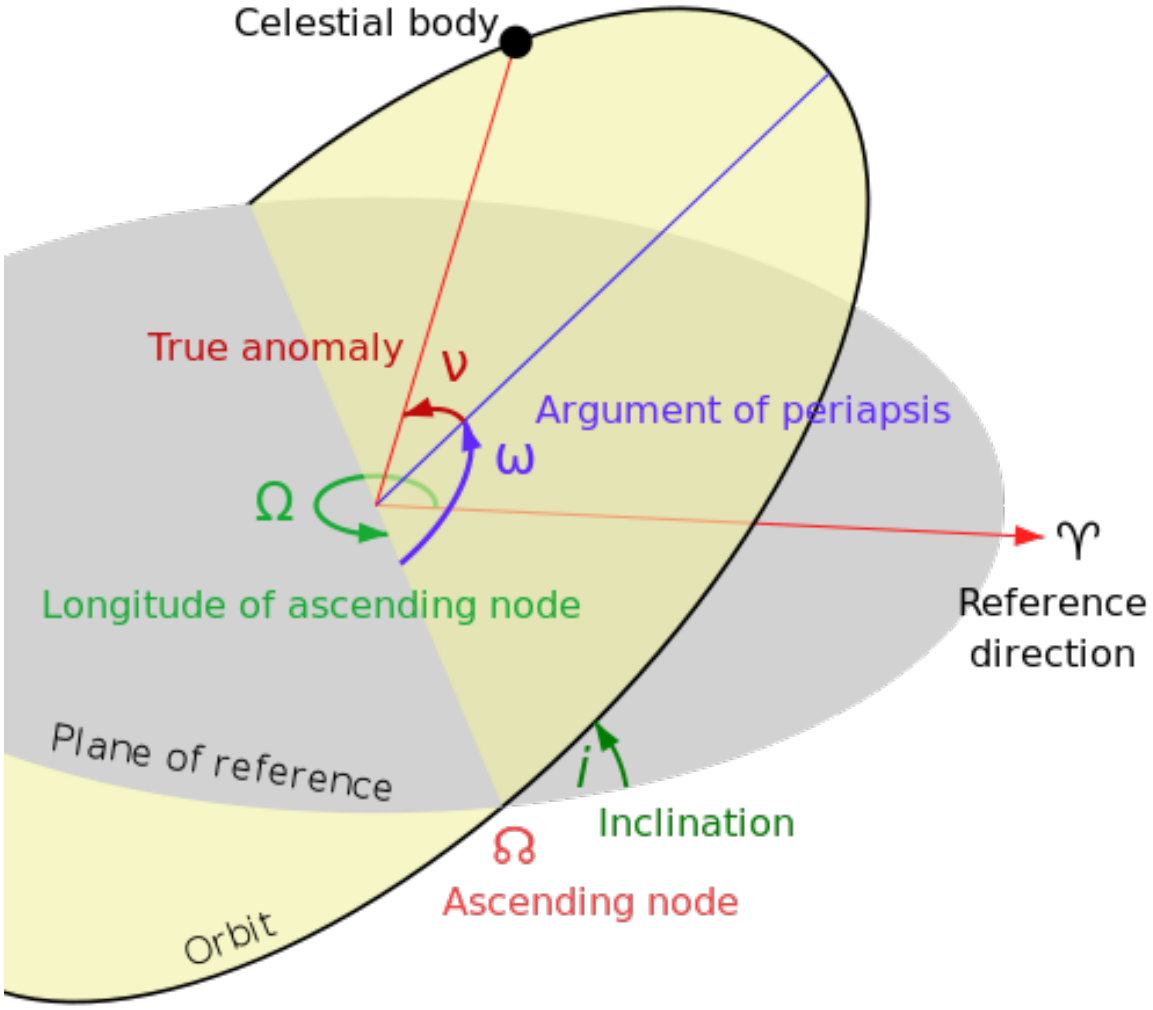

Figure 1. The Kepler elements that describe the motion of a body around a central object. The orbital plane is shown in yellow, and the reference plane is shown in grey. Inclination (i) describes the tilt of the orbit. Longitude of ascending node (Ω) and argument of periapsis (ω) describe the orientation of the orbit. True anomaly (ν) describes the location of the body along its orbit. (Image Credit: https://en.wikipedia.org/wiki/Orbital_elements#/media/File:Orbit1.svg)

ellipse's long axis. *Eccentricity* (e) describes the shape of the orbit, and ranges from 0 to 1. An orbit with $e = 0$ is perfectly circular, and as e increases, the more elongated the orbit becomes. Orbits with eccentricities close to 1 are very elliptical.

Two more useful numbers (though these are not Kepler elements) are the distances of closest and furthest approach of the body to the central object. The body's closest approach to the central object is called periapsis or *pericenter* (r_p), and can be calculated with these first two orbital elements as $r_p = a(1 - e)$. The body's furthest point from the central object is apoapsis or *apocenter*, and is calculated as $r_a = a(1 + e)$.

The next three orbital elements are angles that describe the orientation of the orbit ellipse in space. These angles are defined with respect to a reference plane (usually the equatorial plane of the central object) and a reference direction on the reference plane. *Longitude of ascending node* (Ω) is the angle on the reference plane between the reference direction and the orbit's *ascending node*, where the body crosses the reference plane from below. *Inclination* (i) measures the tilt of the orbital plane with respect to the reference plane, measured at the ascending node. *Argument of periapsis* (ω) is the angle on the orbital plane between the ascending node and the orbit's periapsis.

The last element, *true anomaly* (ν), is the angle on the orbital plane between the orbit's periapsis and the location of the body on the orbit. Together, these six elements are sufficient to fully describe the location of a body at any point in time.

There are two more useful properties of an orbit that we will refer to in subsequent sections. Related to an orbit's inclination is its *out-of-plane inclination*, (i_p). Put simply, i_p measures how much the orbital plane is tilted off of the reference plane. While regular Kepler inclination i must be measured at the ascending node and has some dependence on the other orbital elements, i_p does not, making it a simpler measure of the tilt of an orbit. Due to its simplicity, we will use the out-of-plane inclination instead of the Kepler inclination throughout this work. Lastly is an orbit's *eccentricity vector*, a vector that points from the central object towards the pericenter of the orbit, with a magnitude equal to the eccentricity of the orbit.

2.2. *Dynamical Processes*

Here, we describe the dynamical processes and terms relevant to eccentric nuclear disks and two-population models of stellar clusters. For each term, we first describe the process simply while retaining the information essential to understanding the following material. If applicable, we then include a more technical and detailed discussion for those who are interested and/or familiar with stellar dynamics.

Two-body relaxation. In a star cluster, each individual star feels the force of gravity from not only the central object, but also from every other star in the cluster. When two stars pass close to each other, they interact gravitationally in a *two-body encounter*, in which the stars scatter each other onto new orbits. Over time, the stars of the cluster undergo many two-body encounters, and this spreads out the cluster in a process called *two-body relaxation*.

Secular dynamics. When two-body encounters are rare, stars in the cluster stay on the same orbit for many trips around the central black hole. When this happens, we can describe the interactions between stars using the *secular approximation*. In this approximation, the interactions between stars become orbit-averaged. To do this, we can think of the stars as being spread out along their orbits to produce a collection of massive orbit wires that interact gravitationally. Unlike two-body

encounters, which are random, secular interactions are coherent, adding up to change the orbits of stars predictably over long timescales.

The *Secular dynamical timescale*, or *secular time* for short, is the typical time that it takes for secular effects to have a meaningful effect on a system. This time is given by

$$t_{\rm sec} \equiv \left(\frac{M_\bullet}{M_{\rm disk}}\right) P, \tag{1}$$

where $M_\bullet$ and $M_{\rm disk}$ are the the black hole and disk mass respectively, and P is the orbital period of a star at the inner edge of the disk (Rauch & Tremaine 1996).

Angular Momentum and Torque. Angular momentum is the orbital equivalent to linear momentum. An object travelling in a straight line possesses linear momentum proportional to its mass and velocity. A star orbiting a black hole has *angular momentum*, which is again proportional to its mass and velocity, but also to its distance from the black hole. Stars with lower angular momentum move more slowly, and have higher eccentricities at a given semimajor axis. Just as objects moving in a straight line change their momentum through force, bodies on orbits change their angular momentum through *torque*, the rotational equivalent of force. Torque acting on a body changes its angular momentum and thus the eccentricity (and potentially orientation) of its orbit. When no torque is acting on a body, its angular momentum is conserved.

More precisely, while linear momentum is $\mathbf{p} = m\mathbf{v}$, orbital angular momentum is given by

$$\mathbf{J} = m\mathbf{r} \times \mathbf{v} \tag{2}$$

where m is the body's mass, $\mathbf{r}$ is the position vector of the body pointing from the central object to the body, and $\mathbf{v}$ is the body's velocity vector. Note that the direction of the angular momentum vector is normal (perpendicular) to the orbital plane, following the right-hand-rule. The magnitude of the angular momentum is also given by

$$J = m\sqrt{GMa(1-e^2)} \tag{3}$$

where m and M are the masses of the body and central object, respectively.

Torque is given by

$$\boldsymbol{\tau} = \frac{d\mathbf{J}}{dt} = \mathbf{r} \times \mathbf{F} \tag{4}$$

where $\mathbf{F}$ is the force on the body. In this work, torque is important in the context of secular dynamics, where torques between an orbit and the rest of the END add to radically change the eccentricity of the orbit, as discussed in Section 4.3.1.

Apsidal Precession. In any system that contains more than one star orbiting the black hole, the gravitational forces between the stars cause the orbit wires of the stars to rotate around the central object like clock hands. *Apsidal precession* refers to this rotation of the orbit pericenters around the central body.

This can equivalently be thought of as the eccentricity vector of the orbit rotating slowly around the central object in the orbital plane.

Dynamical Friction. The more massive a star is, the larger its gravitational influence on the other stars in the cluster. Heavy stars moving through a collection of more numerous light stars will experience *dynamical friction*, which can be thought of as gravitational drag, analogous to a baseball

experiencing aerodynamic drag as it moves through a large amount of much lighter air molecules. This effect slows down the heavy stars over time while "slingshotting" the light stars to higher speeds.

Dynamical friction operates through two-body encounters between the heavy star and the lighter stars around it. As a heavy star moves through a "sea" of lighter stars, its gravity pulls the light stars towards it and creates a "wake" of light stars behind it. This wake is more dense than the surrounding cluster, and exerts a net gravitational pull on the heavy star opposite to its direction of motion, slowing it down over time.

Mass Segregation. Put simply, *radial mass segregation* is the tendency of heavier stars to sink towards the center of a cluster while pushing the lighter stars out. In the context of a disk, this means that the heaviest stars concentrate at the inner edge of the disk and the light stars concentrate at the outer edge. *Vertical mass segregation* is a similar process, where heavier stars tend to concentrate closer to the rotation plane of the cluster while pushing light stars above the rotation plane. Applied to a disk, heavier stars will be found on orbits that lie in the disk midplane, while light stars' orbits will be more tilted. Both kinds of mass segregation become weaker as the number of massive stars increases relative to the number of light stars.

Explained more thoroughly, mass segregation is a consequence of two-body relaxation. Two-body encounters tend to equate the kinetic energies of the participant stars. This drives the cluster towards *energy equipartition*, where the kinetic energy of all the stars is equal. Once equipartition is reached, the more (less) massive a star is, the more slowly (quickly) it will be moving. The slower-moving heavy stars will concentrate towards the center of the cluster, and the more quickly-moving light stars will be driven out.

Mass segregation has previously been well-studied in both spherical clusters like that at the center of our Milky Way (e.g. Alexander & Hopman 2009, hereafter AH09; Bahcall & Wolf 1977; Spitzer 1987) and in axisymmetric disks (disks in which the orbits are spread out, as opposed to aligned as they are in ENDs) (Alexander et al. 2007; Mikhaloff & Perets 2017). AH09 found that the strength of the mass segregation can be described by the *relaxational coupling parameter* (Δ), given by

$$\Delta \simeq \frac{N_H M_H^2}{N_L M_L^2} \times \frac{4}{3 + M_H/M_L}, \tag{5}$$

where M_H and M_L are the mass of a heavy and light star, respectively, and N_H and N_L are the number of heavy and light stars respectively.[1]

AH09 also find that mass segregation separates into two strength regimes. In the weak regime ($\Delta \gg 1$), heavy stars are relatively common and interact with both light and other heavy stars. In the strong regime ($\Delta \ll 1$), heavy stars are too rare to scatter each other frequently, and so sink to the center of the cluster primarily through dynamical friction with the larger number of light stars. In summary, fewer heavy stars corresponds to lower values of Δ and stronger mass segregation.

[1] AH09 define Δ as the ratio of the energy–space diffusion coefficients from heavy–heavy interactions to the diffusion coefficients from heavy–light interactions in a Fokker–Planck formalism, but also give this as an equivalent expression.

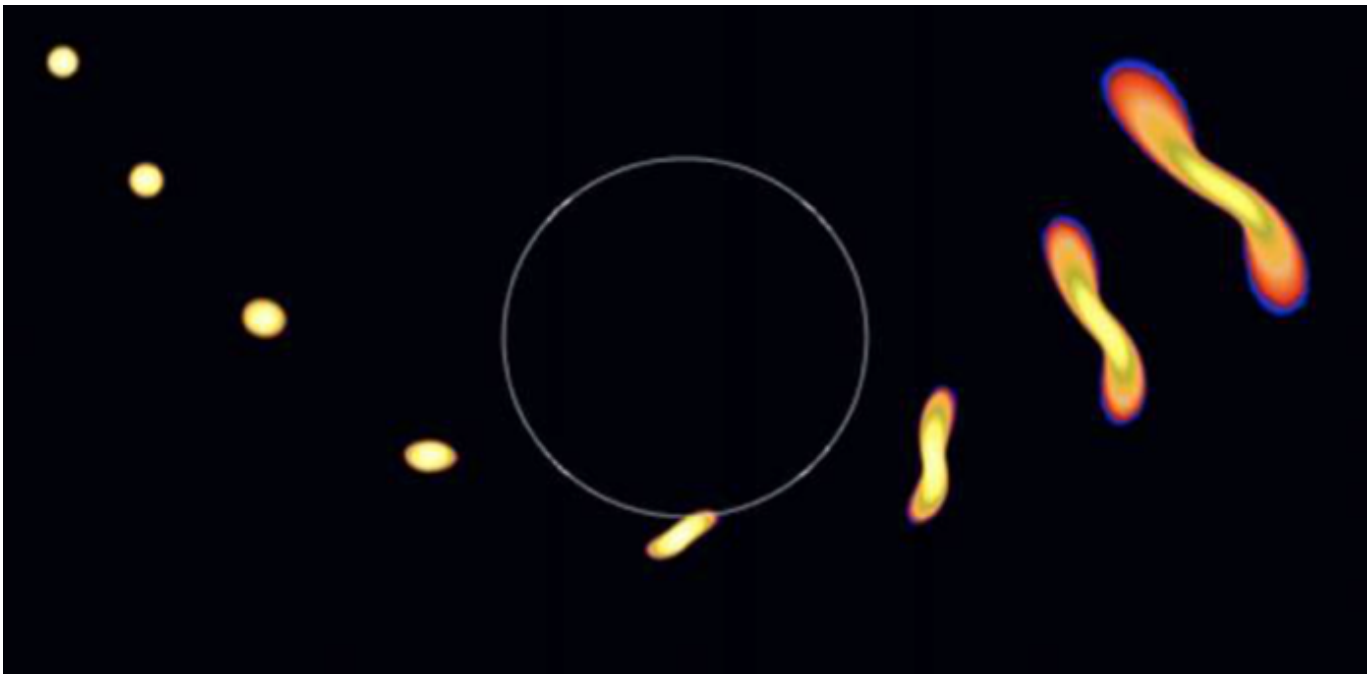

Figure 2. A computer simulation of the tidal disruption of a white dwarf star. The white circle shows the event horizon of the black hole. As the star passes through its pericenter, it is torn apart. The debris forms two streams of gas, called tidal tails. (Adapted from Fig. 4 of Rosswog et al. (2009))

2.3. *Tidal Disruption Events*

In general, the force of gravity between two objects decreases in strength the farther away the two objects are from each other. This difference in strength with distance can also be felt over the size of the objects themselves, as gravity pulls slightly harder on the side of the objects that face each other. The difference in gravity's strength between the near and far side of an object is called the *tidal force*, which has the net effect of stretching the objects it acts upon. Tidal forces are so named because they are responsible for Earth's tides. The tidal force from the Moon on Earth stretches the Earth's oceans towards the Moon, creating slight bulges. As the Earth rotates, these bulges move across its surface, which we experience as the rise and recession of the oceans in two cycles every day. In most systems, including the Earth and Moon, tidal forces are very weak compared to gravity's attraction between the objects.

Near a black hole however, tidal forces become extremely strong. Occasionally, a star orbiting a supermassive black hole at the center of a galaxy may be scattered onto an orbit that takes it very close to the black hole. If the star gets close enough, the tidal forces from the black hole will overcome the gravity holding the star together, and the star is torn apart in a *Tidal Disruption Event* (TDE). The radius at which the tidal force exactly balances the internal gravity of the star is called the black hole's *tidal radius*, given by

$$r_{\rm t} = \left(\frac{M_\bullet}{M_*}\right)^{1/3} R_* \tag{6}$$

where $M_\bullet$ and M_* are the black hole and stellar mass, respectively, and R_* is the star radius (Rees 1988). A star is tidally disrupted when it passes through its pericenter if the pericenter distance, $r_p = a(1-e)$, is less than the tidal radius of the black hole.

Several dozen candidate TDEs have been observed as optical/UV (van Velzen et al. 2011; Gezari et al. 2012; Arcavi et al. 2014; Chornock et al. 2014; Holoien et al. 2016) and soft X–ray (Auchettl et al. 2017 and the references therein) flares from the centers of their host galaxies that are typically observable for several years. These flares are comparable in brightness to supernovae, and are extremely interesting targets for observers.

Figure 2 shows a computer simulation of the tidal disruption of a white dwarf star by Rosswog et al. (2009). The debris from the star is pulled into two long streams of gas. Half of this gas will continue to orbit the black hole, forming a disk of gas that the black hole will slowly swallow up. A large active area of research in astrophysics studies how black holes eat such gas disks in a process called accretion, and TDEs provide natural laboratories for this vein of research (Stone 2015). In addition, TDEs can provide useful tests of the theory of general relativity (i.e. Lu et al. 2017, van Velzen 2018), as well as mass estimates of their host black holes (Stone & Metzger 2016a). For these reasons, TDEs are an emerging area of interest within astrophysics.

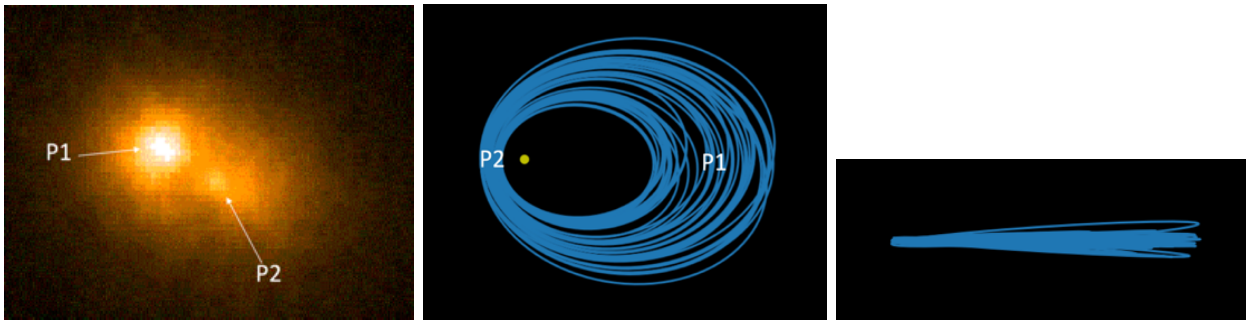

Figure 3. *Left Panel*: An image of the nucleus of the Andromeda Galaxy (Lauer et al. 1993). The two bright spots, P1 and P2, are labeled. Their separation is ~ 2 pc. *Center Panel*: A top-down view schematic of the orbit wires in an END. The yellow dot (not to scale) is the position of the black hole. The regions of the END that produce the bright spots seen in the image are labeled. *Right Panel*: A side view of the END orbit wires. A real END would likely include thousands of stars, but we show only 40 orbits here for clarity.

2.4. *Eccentric Nuclear Disks*

An Eccentric Nuclear Disk (END) is a collection of stars orbiting a supermassive black hole in the center of a galaxy, where the stars lie on aligned, highly eccentric orbits in a thin disk (technically, we say that the orbits are *apsidally aligned*; this means the eccentricity vectors of the orbits all point in the same direction). The closest END to our Milky Way galaxy is in the nucleus of the Andromeda Galaxy (M31) (Tremaine 1995). Figure 3 shows a *Hubble Space Telescope* image of the nucleus of the Andromeda Galaxy, along with a schematic of the orbit wires of an END. The image of M31's nucleus shows two brightness peaks, created by the points of furthest and closest approach of the END's stars to the black hole. Additional observational evidence for the existence of ENDs was presented by Lauer et al. (2005), who showed that up to $\sim 20\%$ of nearby elliptical galaxy nuclei could be ENDs. This evidence along with the presence of an END in our nearest large neighbor galaxy suggests that ENDs may be a common type of galaxy nucleus.

Madigan et al. (2018) helped explain why ENDs might be so common, showing that they are dynamically stable structures that keep themselves together through secular (orbit-averaged) gravitational torques between orbits (see Section 4.3.1 for a detailed description of this process). This

stability mechanism can drive orbits to extremely high eccentricities ($e > 0.999$), resulting in the star dipping below the black hole's tidal radius at its closest approach and producing a TDE. Because stars are driven close to the black hole very efficiently in an END, the TDE rate for a young END can be as frequent as one TDE per year,[2] orders of magnitude higher than estimates of TDE rates from a spherical star cluster like the one at the center of our Milky Way ($\sim 10^{-4}$ yr^{-1} gal^{-1} (Magorrian et al. 1998; Wang & Merritt 2004; Stone & Metzger 2016b)). This suggests a significant fraction of TDEs could come from ENDs. Additionally, many observed TDEs are in post–merger E+A/K+A galaxies (French et al. 2016). This result is consistent with current theories of how ENDs form during galaxy mergers (Hopkins & Quataert 2010), as these young ENDs would produce the high rate of TDEs that we observe from these galaxies.

3. SIMULATIONS

We use N–body simulations to study how stars move in a two-population END. N–body simulations are computer simulations which model the gravitational interaction of particles, or in our case, stars orbiting a supermassive black hole. Each star in the simulation feels the force of gravity from every other star in the simulation as well as the black hole, making this the most realistic and detailed method currently available for studying clusters of stars.

We use the N–Body code `REBOUND` (Rein & Liu 2012) with the IAS15 adaptive-timestep integrator (Rein & Spiegel 2015) to simulate an END. Following the example of AH09, we use two populations of stars to study mass segregation in ENDs, where each heavy star is ten times as massive as a light star, $M_H = 10\ M_L$. This two-population model is a reasonable approximation of an evolved star cluster, where the light stars in our simulations represent old main–sequence stars, white dwarfs, and neutron stars of order one solar mass, and the heavy stars represent stellar–mass black holes of order ten solar masses.

We vary two quantities in our simulations: (i) the number of heavy stars, N_H, and (ii) their initial inclination distribution, i_H. We refer to simulations where the former (latter) is varied as "N_H-vary" ("i_H-vary"). The "N_H-vary" set aims to explore how changing the strength of the mass segregation affects the dynamics of the disk and the TDE rate of each population of stars. The "i_H-vary" set studies how vertical mass segregation is affected when the orbits of heavy stars are initially tilted above the plane of the disk.

All simulations are run for the time it takes a star at the inner edge of the disk to complete 500 orbits. For better statistics we run ∼40 simulations for each set of parameters.[3] We summarize the simulation parameters in Table 1.

In our simulations, we use a special set of units that allows our simulations to be scaled to different realistic black hole masses and disk sizes. The semimajor axis of the innermost orbit, the black hole's mass, and the gravitational constant are all 1, such that the orbital period at the inner edge of the disk is 2π. All stars initially have semimajor axes between 1 and 2 with decreasing frequency towards the outer edge of the disk (more precisely, with a surface density profile $\Sigma \propto a^{-2}$), and eccentricities of 0.7. All figures in this work that present simulation data will be in simulation units. The total disk mass is one percent of the black hole's mass, and there are 400 light stars.

[2] Although if disruptions really occur once per year, the black hole may not return to quiescence between disruptions, and such events would not currently be identified as TDEs. Instead, these nuclei would likely be classified as Active Galactic Nuclei.

[3] The precise number of simulations varies as simulations sometimes stall due to formation of binary systems.

Table 1. Initial conditions for our N–body simulations. There are two main sets of simulations, broken down into groups that share initial conditions. For each group, we list the number of simulations, the spread (three times the standard deviation, σ) of the orbit inclinations (rotation angles θ_a and θ_l described in § 3), the number of heavy stars (N_H), and the resulting coupling parameter (Δ; see eq 5 and the surrounding discussion). Each simulation has 400 light stars. The standard deviation of the third orbit rotation angle (θ_j) is three degrees.

Simulation Set	Simulation Group	Number of Simulations in Group	Inclination Spread $(3\sigma_{\theta_a}, 3\sigma_{\theta_l})$ of Heavy Stars [degrees]	Inclination Spread $(3\sigma_{\theta_a}, 3\sigma_{\theta_l})$ of Light Stars [degrees]	N_H	Δ
N_H-vary	$N_H = 5$	35	5	5	5	0.384
	$N_H = 10$	44	"	"	10	0.769
	$N_H = 15$	33	"	"	15	1.15
	$N_H = 20$	39	"	"	20	1.54
	$N_H = 25$	43	"	"	25	1.92
	$N_H = 30$	38	"	"	30	2.31
	$N_H = 35$	42	"	"	35	2.69
	$N_H = 40$	39	"	"	40	3.08
i_H-vary	$i_H = 5$	10	5	5	25	1.92
	$i_H = 10$	10	10	"	25	1.92
	$i_H = 15$	10	15	"	25	1.92
	$i_H = 20$	10	20	"	25	1.92
	$i_H = 25$	10	25	"	25	1.92
	control	10	-	"	0	-

We initialize orbits with the same orientation, and then introduce a small scatter (a few degrees at most) in the orientation of each orbit before starting the simulation. For the interested reader, the exact procedure is as follows: Orbits are created with initially aligned eccentricity and angular momentum vectors. We then introduce a small scatter in these vectors via three rotations. We draw three random angles (θ_a, θ_l, and θ_j) from a normal distribution with a standard deviation of a few degrees (see Table 1 for details). We then rotate the angular momentum vector about the orbit's major axis by θ_a, the angular momentum vector about the latus rectum by θ_l, and the eccentricity vector about the angular momentum vector by θ_j. After initializing the orbits, we search for binary systems, and remove one of their stars in order to increase integration speed. The number of stars removed is of order 5 in each simulation.

To detect TDEs, we use `REBOUND`'s built-in collision detection capability. To set a tidal radius we have to set an overall length scale for the simulations; we choose the inner edge of the disk ($a = 1$) to be at 0.05 pc. Then the supermassive black hole is given a radius equal to the tidal radius of a sun-like star around a 10^7 solar mass black hole, which is 1.5×10^8 km (or 9.694×10^{-5} in simulation units).

If `REBOUND` detects that a star has come within the tidal radius of the black hole particle, we record a TDE. The stars that disrupt are not removed from the simulation and are allowed to continue on

their orbits, however if they disrupt more than once, we do not count the subsequent disruption(s) in our analysis. We keep disrupted stars to simplify analysis and to keep the disk as constant as possible through the simulation.

For simplicity, we take the tidal radius to be the same for light and heavy stars in our initial analysis. We discuss how the tidal radius would vary as a function of stellar properties in Section 5.1 and the effect this would have on TDE rates.

Choosing real-world values for the black hole mass and length scale of the disk means that we can also define a timescale for our simulations by using Kepler's third law. One orbital period at the inner edge of the disk (P) is 331.4 years. The secular timescale is then about 33,000 years, and a simulation runs for just under 166,000 years.

It is important to note that including two stellar masses is a useful step towards realism, however our simulations include too few stars to be considered realistic. We use low particle numbers due to computational limitations, though a real END could have tens of thousands of stars. The ratio of the disk mass to black hole mass (10^{-2}) affects the dynamics of the disk[4], so we choose to keep this constant between the simulations for consistency. Thus, our heavy (light) star particles have masses of order 10^{-4} (10^{-5}) times the black hole mass, though the precise masses vary based on the number of heavy stars in a particular simulation. Our stars are therefore much more massive than what is realistic, which causes two–body interactions in our simulations to be stronger than in realistic disks. My collaborators quantified the effect of this stronger two-body relaxation in our simulations, and used a different model to extend our results to systems with realistic numbers of stars (See Section 3.4 of Foote et al. 2020).

4. RESULTS

4.1. *Radial Mass Segregation*

As in spherical clusters and axisymmetric disks, we find that ENDs show both strong and weak radial mass segregation, by which heavy stars sink to the inner edge of the disk while scattering light stars out. Figure 4 shows the semimajor axis evolution for simulations with different numbers of heavy stars ("N_H-vary" in Table 1).

Simulations with five heavy stars are in the strong regime, where massive stars actively sink to the center of the cluster. All other simulations are in the weak regime, where the heavy stars simply reach lower semimajor axes than the light stars. The Δ cutoff between the strong and weak regime in ENDs is thus likely between 0.4 and 0.8, consistent with previous results from spherical clusters ($\Delta \approx 1$).

4.2. *Vertical Mass Segregation*

We find that stars in ENDs also undergo vertical mass segregation in which heavy stars orbit in the midplane of the disk, while light stars are more likely to have higher inclinations. Figure 5 shows the evolution of the out-of-plane inclination for both populations of stars in each simulation group from the N_H-vary set. Recall that out-of-plane inclination measures how tilted an orbit is with respect to the midplane of the disk.

[4] Specifically, it affects precession of the disk orbits. More massive disks have faster precession and shorter secular timescales, but if the disk is too massive the black hole's gravity will no longer be the dominant force on the stars, and the disk would not be stable. Our choice of disk to black hole mass ratio provides a good balance between disk stability and a short enough secular time that our disks evolve significantly over the course of a simulation.

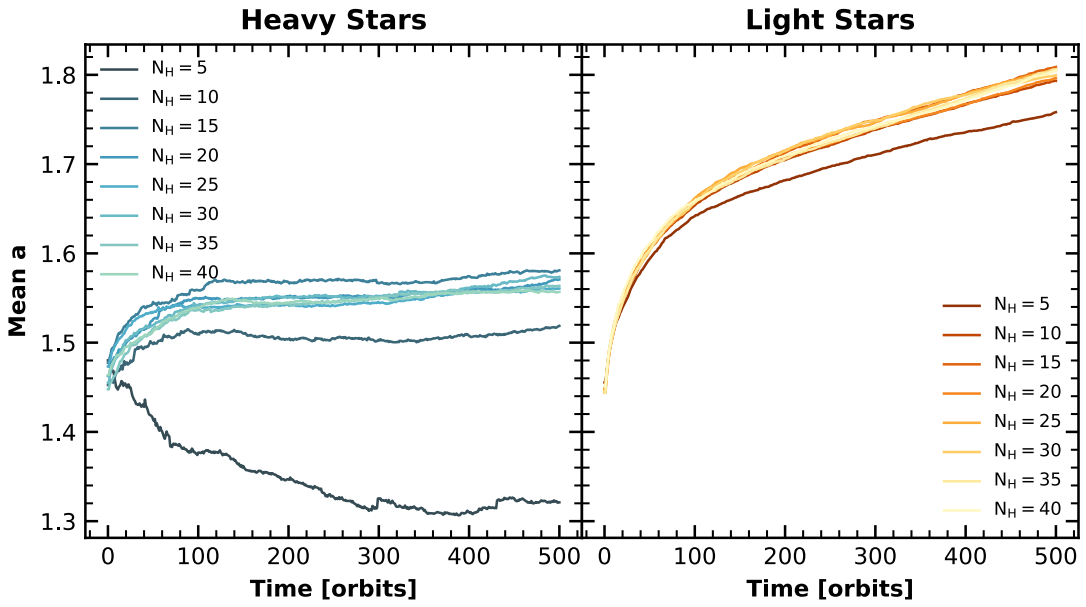

Figure 4. *Left panel:* Mean semimajor axis of the heavy and light populations as a function of time for simulations with different numbers of heavy stars ("N_H-vary" from Table 1). Each line is the mean semimajor axis of all stars from all of the simulations in the group. Simulations with five heavy stars are clearly separated from the rest, suggesting the presence of weak and strong mass segregation regimes as in spherical star clusters. *Right panel:* Mean semimajor axis of the light population as a function of time for the same simulations.

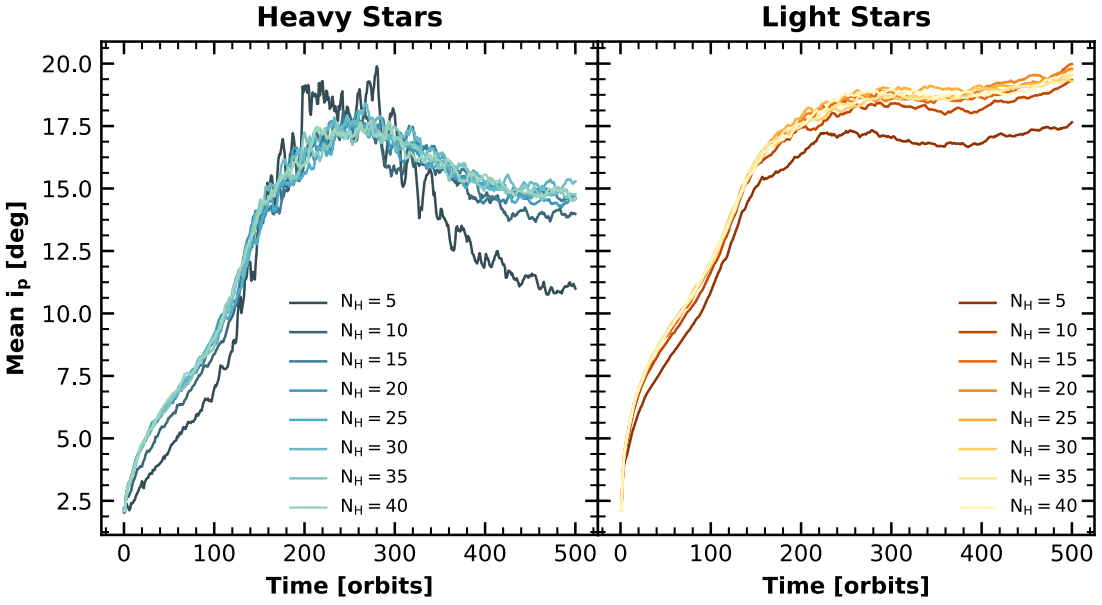

Figure 5. Mean out-of-plane inclination of the heavy and light populations as a function of time for simulations with different numbers of heavy stars ("N_H-vary" from Table 1). Each line is the mean out-of-plane inclination of all stars from all of the simulations in the group. Vertical mass segregation occurs after two secular times ($\sim$ 200 orbital periods). As with radial segregation, vertical segregation shows both strong and weak regimes.

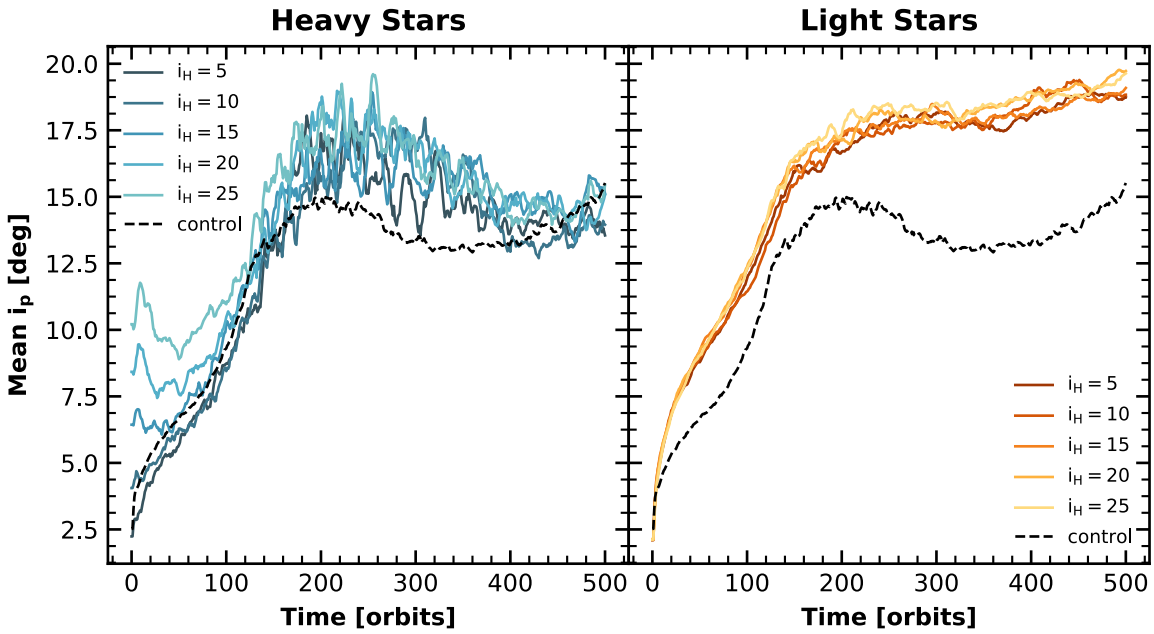

Figure 6. Mean out-of plane inclination versus time for simulations with different initial heavy star inclinations (the "i_H-vary" simulations in Table 1). Each solid line is the mean out-of-plane inclination of all stars from all of the simulations in the group. The dashed line shows the mean out-of-plane inclination in simulations with no heavy stars. *Left Panel*: The heavy stars relax to roughly the same inclination after ~ 150 orbital periods, regardless of their initial inclinations. *Right Panel*: The light stars do not show any dependence on the initial conditions.

As with radial mass segregation, vertical mass segregation shows both a strong and weak regime. In simulations with the fewest heavy stars, the heavy population shows much stronger segregation than in other simulation groups. We also explore how resistant vertical mass segregation is to changes in the initial conditions by varying the initial inclination distribution of the heavy stars. These simulations ("i_H-vary" in Table 1) use 25 heavy stars each, placing them in the weak mass segregation regime. Each group of simulations in this set uses a different spread for the initial tilt of the heavy star orbits.

Figure 6 shows the mean i_p of each group in the "i_H-vary" set. Heavy stars drop to low inclinations very quickly, with the simulation groups becoming very similar between 100 and 150 orbital periods, which is of order the secular time. Our choice of Δ for this set ensures that the overall inclination behavior we observe will also be qualitatively valid in the strong regime, where the mass segregation will be only be more effective at dropping the inclinations of the heavy stars. Thus, after a few secular times, we expect to find heavy stars in an END preferentially at lower inclinations than light stars.

In order to more clearly show the difference between the two populations, Figure 7 condenses the different simulation groups from Figure 6, showing the mean and standard deviation of i_p for all stars in the entire "i_H-vary" set. This figure shows that despite starting at high inclinations, heavy stars drop to lower inclinations than the light stars on a timescale of ~ 20 orbital periods, and remain at lower inclinations than light stars on average for the remainder of the simulation. The initial violent drop in heavy star inclinations is due to two-body relaxation being stronger in our simulations than what is realistic.

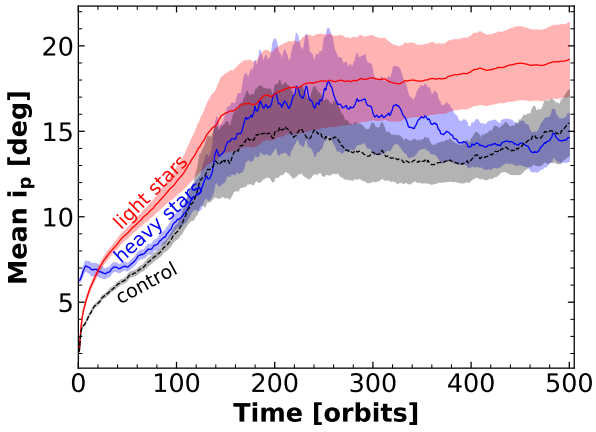

Figure 7. Mean out-of-plane inclination for the simulations with different initial heavy star inclinations ("i_H-vary" from Table 1). Each line shows the mean and standard deviation of i_p for all of the stars from all of the simulations in the entire i_H-vary set. The blue line shows the heavy stars, the red line shows the light stars, and the dashed line shows the control simulations. The heavy stars behave more like the control stars, while they scatter the light stars to higher inclinations than they would reach without heavy stars present.

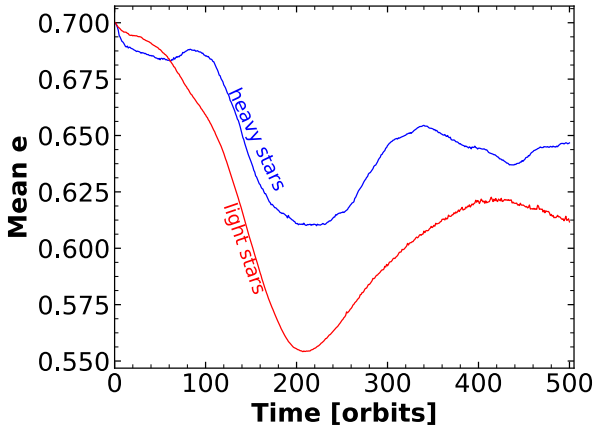

Figure 8. Mean eccentricity for the light and heavy stars in simulations that have different initial heavy star inclinations("i_H-vary" from Table 1). Each line shows the mean of e for all of the stars from all of the simulations in the entire i_H-vary set. As the inclination of both populations increases (Figure 7), the eccentricity of both populations decreases after one secular time. Whereas two-body interactions would cause both inclination and eccentricity to increase, this opposite evolution of inclination and eccentricity is characteristic of secular effects.

Despite artificially strong two–body relaxation, we can still use these N–body simulations to show that secular effects play an important role in the inclination evolution of ENDs. Figure 8 shows the eccentricity evolution of both populations shown in Figure 7. If vertical mass segregation was driven purely by two-body interactions, we would expect both the inclination and eccentricity to increase over time as the disk relaxes (e.g. Stewart & Ida 2000). Instead, as the inclination of both populations increases, the eccentricity of both populations decreases after one secular time. This opposite (and smooth) evolution of eccentricity and inclination is a result of angular momentum conservation and is characteristic of secular dynamics. This suggests that vertical mass segregation (unlike radial mass segregation, which is purely a two-body effect) is driven at least partially by orbit-averaged dynamics.

4.3. *TDEs*

In this section, we first present a discussion of why ENDs cause so many TDEs compared to other clusters, and then discuss the results of our simulations with regard to TDEs.

4.3.1. *How do ENDs Cause so Many TDEs?*

ENDs are exciting objects of study in large part because they have a TDE rate up to 3 or 4 orders of magnitude higher than what would be expected from other types of star clusters. Before presenting our results with regard to TDE rates, it is necessary to explain why ENDs throw so many stars

towards their central black holes. The following discussion is adapted from Madigan et al. (2018), who first explained this property of ENDs.

ENDs keep themselves stable through secular torques between the disk orbits. The orbits of an END undergo apsidal precession, where the orbit wires rotate coherently around the black hole like clock hands, on timescales of many orbital periods of the stars. In a stable END, this precession is *prograde*–in the same direction that the stars move on their orbits. For example, if the stars orbit counterclockwise as seen from above the disk, the orbit wires rotate counterclockwise as well.

If any orbit precesses ahead of the rest of the disk, it will begin to feel a gravitational force from the collection of disk stars that it has left behind. This force manifests as a secular torque on the orbit wire, which decreases the angular momentum of the orbit, raising its eccentricity. More eccentric orbits precess more slowly, so the orbit slows its precession rate and allows the rest of the disk to catch back up to it. Similarly, if an orbit lags behind the disk, the torque lowers its eccentricity, the orbit precesses more quickly, and catches back up with the disk. In this manner, the disk structure is kept stable.

ENDs produce such a high rate of TDEs because of this stability mechanism. As orbits that move ahead of the disk have their eccentricities raised, their pericenters, given by $r_p = a(1-e)$, drop closer and closer to the tidal radius, and in some cases dip below it. When an orbit's pericenter is below the tidal radius, the star is tidally disrupted when it passes through its closest approach to the black hole. Figure 9 shows this process, or how an orbit that precesses ahead of the disk leads to a TDE. In summary, TDEs are a direct consequence of the method by which ENDs are kept stable. In other types of clusters, TDEs require a two-body encounter to randomly place a star on an orbit that takes it within the tidal radius, but in an END, stars are systematically funneled towards the black hole.

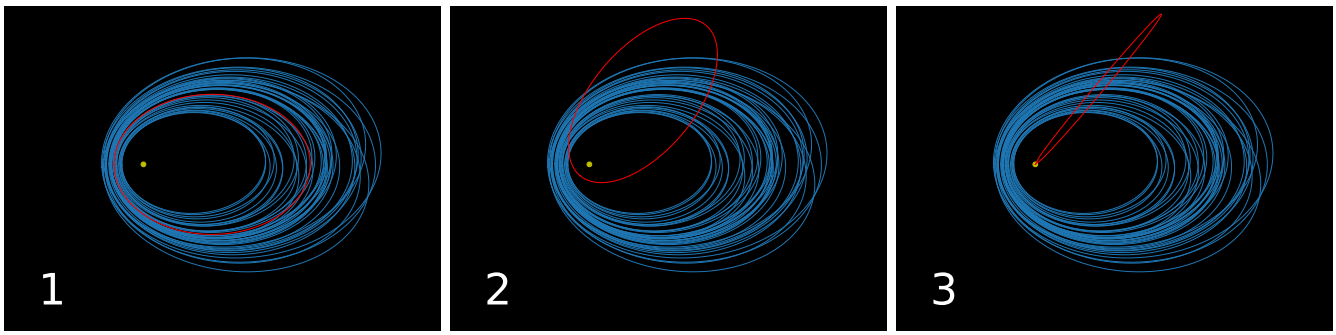

Figure 9. Schematics showing how ENDs produce TDEs. In these diagrams, the orbits precesses counterclockwise, and the view rotates with the disk. (1) An orbit, highlighted in red, starts in the disk. (2) The highlighted orbit precesses ahead of the disk. (3) Secular torques dramatically raise the eccentricity of the orbit, and the orbit's pericenter drops below the black hole's tidal radius. The star will be tidally disrupted as it passes through its pericenter.

Another relevant feature of a stable END is their *negative eccentricity gradient*, which means that orbits with lower semimajor axes tend to have higher equilibrium eccentricities. An orbit's equilibrium eccentricity is the eccentricity at which the orbit will precess at the same speed as the rest of the disk. In an END, an orbit precesses faster if it has a low semimajor axis and/or low eccentricity. Thus, a low semimajor axis orbit must have a higher equilibrium eccentricity if it is to precess at the same rate as a high semimajor axis orbit. The gradient is developed over a secular time as the stability mechanism operates.

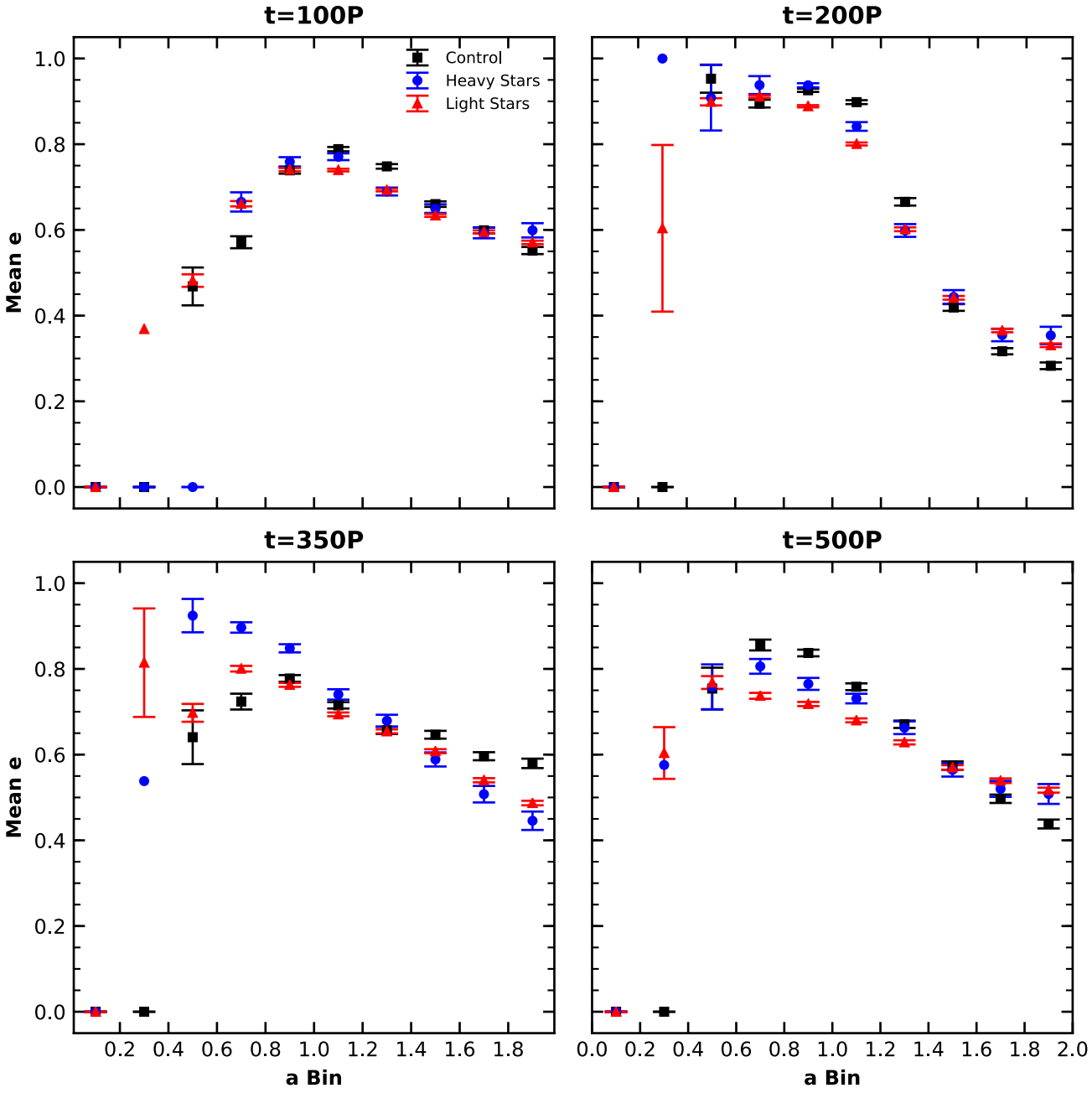

Figure 10. Development of the eccentricity gradient in simulations with different initial heavy star inclinations ("i_H-vary" from Table 1). At the beginning of the simulation, $t = 0$, the eccentricity distribution of all stars is flat at $e = 0.7$. Each panel shows the mean of the eccentricities of stars from all of the simulations in the i_H-vary set in bins of semimajor axis, broken down by population. Error bars show the standard error of the mean. Bins that show an eccentricity of 0 contain no stars at the selected time. *Top Left Panel*: By one secular time, the eccentricity gradient has started to take shape. *Other Panels*: Over the course of the simulation, the gradient changes shape slightly, but the heavy stars always have higher eccentricities than the light stars on average in bins where the bulk of TDEs come from, between a=0.6 and a=1.2.

Now that we know why ENDs cause so many TDEs, we will explain what we expect for TDE rates in our simulations based on the dynamics of a two-population END that we have already discussed. Previous studies of ENDs found that stars at the inner edge of the disk are preferentially disrupted, as they have higher eccentricities (and lower angular momentum) due to the negative eccentricity gradient in ENDs. Higher eccentricity (lower angular momentum) stars are more easily torqued to a high enough eccentricity to disrupt (Madigan et al. 2018). In our two-population simulations, heavy stars tend to have lower semimajor axes (and hence higher eccentricities) than light stars due to radial mass segregation, so we should expect to see a larger fraction of heavy stars disrupting than light stars.

Vertical mass segregation is important too, dropping the heavy stars to lower inclinations than the light stars. For low inclination orbits, the torque from the disk changes their eccentricity rather than their orbital orientation. Thus, heavy stars are raised to higher eccentricities than the light stars even at a fixed semimajor axis. This can be seen in Figure 10. This figure shows the development of the eccentricity gradient in eccentric disks with and without two populations. While the shape of the gradient changes over the course of the simulations, the heavy stars always have higher mean eccentricities than light stars between semimajor axes of 0.6 and 1.2. The vast majority of orbits that lead to tidal disruption also have semimajor axes in this range, confirming that heavy stars should be easier to disrupt than light stars at any given semimajor axis.

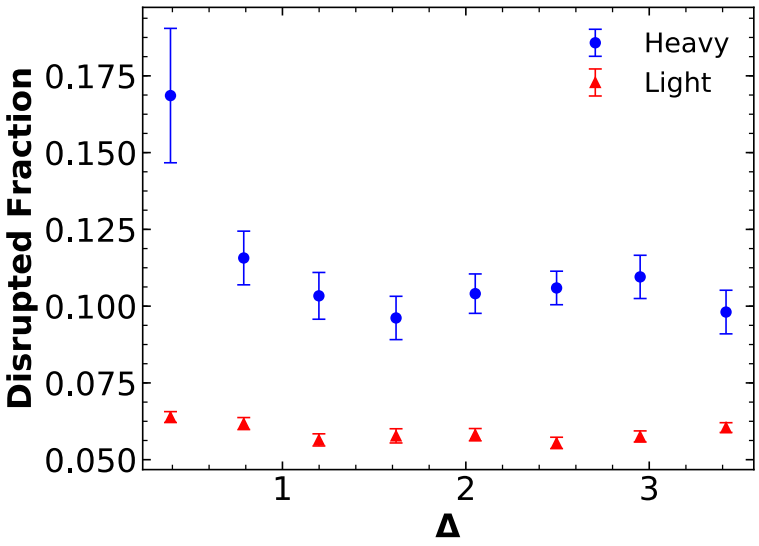

Figure 11. Disrupted fraction vs Δ (or mass segregation strength, lower Δ is stronger mass segregation) for simulations with different numbers of heavy stars ("N_H-vary" from Table 1). Each point shows the mean disrupted fraction for all simulations in a group, broken down into heavy and light stars. Error bars show the standard error of the mean. The disruption rate for light stars is independent of Δ, while heavy star disruption rate increases at low Δ (due to stronger mass segregation).

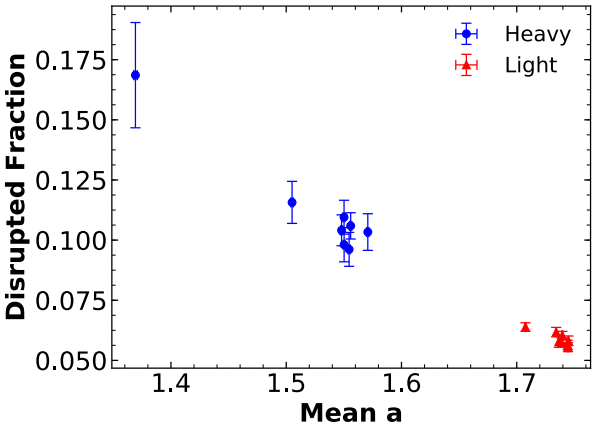

Figure 12. Disrupted fraction vs mean semimajor axis for simulations with different numbers of heavy stars ("N_H-vary" from Table 1). Horizontal axis values are obtained by taking the mean of all stars in all simulations from a group during all timesteps after the first 100 orbital periods. We consider times after 100 orbital periods to allow the disk a full secular time to relax. Horizontal error bars showing the standard error of this mean are included, but are generally smaller than the points. Populations spending more time at low semimajor axes have a correspondingly higher disrupted fraction.

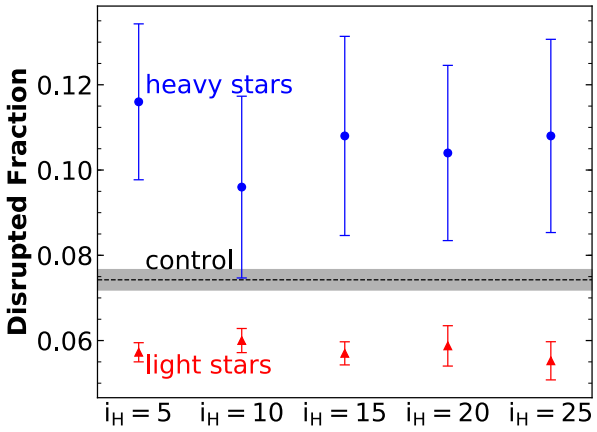

Figure 13. Disrupted fraction for simulations with different initial heavy star inclinations ("i_H-vary" in Table 1). Each point shows the mean of the disrupted fraction from the simulations in the group, with heavy stars shown in blue and light stars shown in red. The errorbars are the standard error of the mean for each simulation group. The dashed line shows the TDE rate per star of the control simulations. The TDE rate is a weak function of the initial inclination, with the heavy star disrupted fraction always exceeding the light star disrupted fraction.

4.3.2. *TDE Rates in Two-Population ENDs*

Here, we present the TDE rate results from our simulations. In order to quantify the TDE rate of each population, we use the *disrupted fraction*, or the number of stars from a population that disrupt during the simulation divided by the total number of stars in that population. Figure 11 shows the disrupted fraction for both populations in simulation groups with different numbers of heavy and light stars ("N_H-vary" in Table 1). Fewer heavy stars (lower Δ) translates to stronger mass segregation, and the group's heavy stars being closer to the inner edge of the disk at higher eccentricity. In all cases, the disrupted fraction of the heavy stars is larger than that of the light stars as expected. In particular, the heavy stars in the most strongly segregated group with $\Delta = 0.384$ have the smallest mean semimajor axis and are the most likely to be disrupted.

Figure 12 again shows the disrupted fraction for each population from the N_H-vary set (similarly to Figure 11), but now as a function of the time- and star-averaged semimajor axis of the population.[5] Populations with a lower mean semimajor axis have a correspondingly higher disrupted fraction.

Figure 13 shows the disrupted fraction of each population for simulations with different initial heavy star inclinations ("i_H-vary" in Table 1). Once again the fraction of heavy stars that are disrupted is larger than the fraction of light stars. There is no significant difference between the groups because

[5] Time averages are taken between $t = 100P$ and the end of the simulation. This is done to allow the disk a secular time to relax, as the TDEs do not begin to happen until after one secular time.

they all have the same Δ, and show the same degree of vertical mass segregation. In particular, the heavy stars from different simulation groups have all reached the same inclination by the time the TDEs begin to occur.

To summarize, in order to be disrupted, a star's orbit must have a torque applied to it to raise it to very high eccentricity. Stars at lower semimajor axes should be easier to disrupt because they need less torque due to their higher equilibrium eccentricity, and stars at low inclination should be easier to disrupt because the torque from the disk changes their orbital eccentricities rather than their orientations. Radial mass segregation places heavy stars at low semimajor axes, and vertical mass segregation places stars at low inclinations. Across all of our simulations, a larger fraction of heavy stars are disrupted, as we would expect.

5. DISCUSSION

In this section, we present a discussion of our results in a wider astrophysical context. In a real END, different stars have different tidal radii, so we explore the effect that this would have on TDE rates. Additionally, we speculate on how many heavy and light stars would likely be present in a real END, including likely Δ values and the resulting mass segregation and structure of the disk. Lastly, we consider the effect that a different initial eccentricity would have on TDE rates.

5.1. *Effects of Star Type on TDE Rates*

Both heavy and light stars have the same tidal radius in our simulations. In reality, the tidal radius depends on quantities such as the stellar mass, radius, and spin (Rees 1988; Golightly et al. 2019). Also, compact objects such as neutron stars and stellar-mass black holes (represented in our simulations by the heavy star particles) are extremely dense and will not be tidally disrupted by the central supermassive black hole, although they can be captured if they pass too close to it.

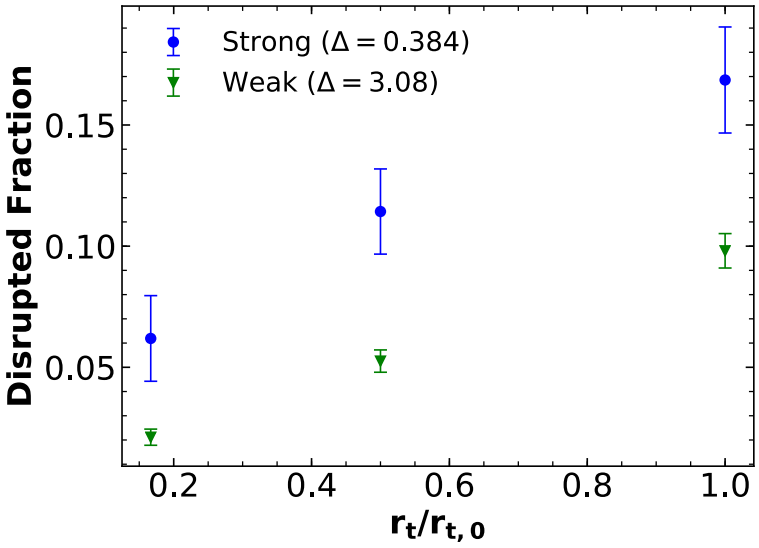

Figure 14. Mean disrupted fraction of heavy stars vs. tidal radius, for two simulation groups, one in each mass segregation regime from the N_H-vary set. $r_{t,0}$ is the tidal radius of a light star. The disrupted fraction is linear with the tidal radius in both cases.

These captures could produce gravitational waves of a frequency that will be observable with future detectors such as the upcoming *Laser Interferometer Space Antenna* (Amaro-Seoane et al. 2017).

In an END, when orbits' pericenters drop below the tidal radius, they stop at a random distance from the black hole (Madigan et al. 2018, Wernke & Madigan 2019). Therefore, we expect the TDE rate to scale linearly with the tidal radius. By screening out heavy TDEs with pericenters above other values of r_t, we can see how the disrupted fraction of heavy objects changes with the tidal radius. Figure 14 shows that the disrupted fraction indeed scales linearly with the tidal radius in our simulations. In a real END, high-mass stars (of order 10 solar masses, comparable to the heavy stars in our simulations) will exist at early times, and will have larger tidal radii than light stars.

A full exploration of how stellar properties and the presence of compact objects translates into observable TDEs and gravitational wave bursts would require including stellar evolution in our simulations. However, my collaborators give a more detailed discussion of this, as well as the effect of the supermassive black hole's properties on TDE rates, which may be found in section 4.1 of Foote et al. (2020).

5.2. *What is the Stellar Make-up of Real ENDs?*

A real END would of course contain far more than two stellar masses, including a spectrum of stars of all masses as well as their remnants (white dwarfs, neutron stars, and stellar mass black holes). A cluster's *mass function* describes how many of each type (mass) of star exist in the cluster. As discussed by AH09, the two-population approximation we use here falls naturally out of "universal" mass functions developed by Salpeter (1955), Miller & Scalo (1979), and Kroupa (2001). After clusters formed with these mass functions evolve, they generally have $\Delta < 0.1$ (AH09), placing them firmly in the strong mass segregation regime. Merritt (2013) shows that a population evolving from the Kroupa mass function reaches $\Delta \approx 0.05$, again in the strong regime.

However, there is also evidence to suggest that star formation and mass functions in galactic nuclei near supermassive black holes may be different from the aforementioned "universal" mass functions used for stars elsewhere in galaxies (e.g. Levin & Beloborodov 2003; Milosavljević & Loeb 2004; Paumard et al. 2006; Levin 2007; Bartko et al. 2010; Lu et al. 2013).

ENDs in particular should also have different mass functions depending on whether the disk stars were formed on eccentric orbits, or if the disk was formed dynamically (e.g. during a galactic merger) after the stars were formed. ENDs formed dynamically from stellar populations with universal mass functions would have $\Delta < 0.1$ as previously discussed, placing them in the strong segregation regime. Conversely, ENDs formed from an initially eccentric thin gas cloud around the supermassive black hole could have more heavy stars than these universal models would predict. Alexander et al. (2008) used computer simulations to study the behavior of initially eccentric gas disks around supermassive black holes. They found that smaller, loosely-bound gas clumps that formed in the disk were particularly vulnerable to tidal disruption at closest approach to the black hole, leading to only the high-mass, dense clumps surviving. Extending their results to star formation, these gas disks would form a larger proportion of heavy stars. It is difficult to predict what Δ would look like in this situation, but we can say it would likely be higher than in other situations, that is $\Delta > 0.1$. Thus, ENDs formed from an initially eccentric gas disk would likely be more weakly segregated than ENDs formed dynamically from existing stars.

The present-day mass function of an END would depend on a myriad of factors, including the formation history of the disk. The age of the disk is also very important, as it affects the mass function through stellar evolution and loss of disk stars to TDEs and captures over time.

Lastly, we note that for most reasonable mass functions, there are many more light stars than heavy stars (Kroupa et al. 2013). Thus, while our results suggest a factor of 2-3 enhancement in the disrupted fraction of heavy stars compared to light stars, TDEs from light stars will still dominate the overall TDE rate of the END.

5.3. *The Effect of Eccentricity*

So far, we have only considered initial eccentricities of $e = 0.7$ in our simulations. Here, we briefly discuss the effect that changing the initial eccentricity has on TDE rates.

In principle, increasing the mean eccentricity of the disk should increase the TDE rate for both populations as all orbits are more eccentric on average. Similarly, decreasing the mean eccentricity of the disk should decrease the TDE rates for both populations.

In order to test this prediction, we use a third small set of simulations. In this third set, we start both populations with the same Δ and inclination distribution, but change the initial eccentricity of the disk orbits. Each simulation contains 25 heavy stars for easy comparison with the i_H-vary set, and there are ten individual simulations for each eccentricity considered.

The left panel of Figure 15 shows the mean disrupted fraction for both populations at each initial eccentricity for this set. The disrupted fraction for both populations increases with the initial eccentricity as expected. This trend is consistent with Madigan et al. (2018), who found that as an END loses mass through disrupted stars, the average eccentricity of the disk drops and the TDE rate is lowered. The right panel of Figure 15 shows that the enhancement of the heavy star disrupted fraction increases weakly with the initial eccentricity.

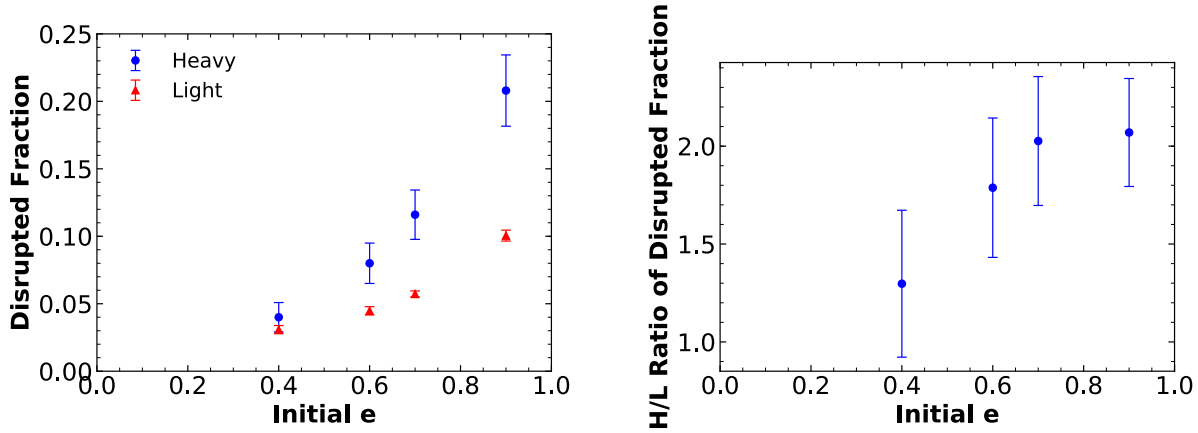

Figure 15. Disrupted fraction for simulations with different initial eccentricities. *Left Panel*: Each point shows the mean of the disrupted fraction from the simulations in the group, with heavy stars shown in blue and light stars shown in red. The errorbars are the standard error of the mean for each simulation group. The disrupted fraction of both populations is correlated with the initial eccentricity of the disk orbits. *Right Panel*: The ratio of the heavy disrupted fraction to light disrupted fraction vs. the initial eccentricity. The enhancement of the heavy specific TDE rate is also correlated with the initial eccentricity.

6. SUMMARY

In this paper, we presented the first study of an eccentric nuclear disk with two stellar populations. Here, we give a summary of our results and their implications.

1. *Radial Mass Segregation*: Similar to previous studies with spherical clusters and axisymmetric disks, two-population ENDs undergo radial mass segregation. The strength of the mass segregation falls into two regimes, determined by the relaxational coupling parameter Δ. The cutoff between the strong and weak segregation occurs around $\Delta \sim 1$.

2. *Vertical Mass Segregation*: In a two-population eccentric disk, heavy stars sink to lower inclinations than light stars on average. This process is highly resistant to artificially raising the inclinations of the heavy stars in our simulations (though these simulations do have artificially strong two-body relaxation). As with radial mass segregation, vertical mass segregation has both a weak and strong regime.

3. *TDE rates*: The negative eccentricity gradient in stable eccentric disks causes stars at low semimajor axes to have higher equilibrium eccentricities, where they are more easily driven onto orbits that take the star within the tidal radius of the supermassive black hole. Stars at low inclinations have their eccentricities altered by secular torques rather than their orientations, leading to these orbits reaching higher eccentricities where they are more susceptible to disruption. Heavy stars are preferentially found at low semimajor axes and low inclinations due to mass segregation, and are more likely to be disrupted than light stars.

   Mass segregation can increase the disrupted fraction of heavy stars in an END by a factor of 2–3 relative to light stars, assuming the same tidal radius for both types of star. Due to the much larger number of light stars, TDEs from light stars will still dominate the overall TDE rate of the END. In a real system, the ratio of the heavy to light star disrupted fraction depends on the age of the disk, as stellar evolution will affect the numbers of each type of star. This also depends on other factors such as the supermassive black hole properties. The larger tidal radii of massive stars will further enhance their TDE rate.

Finally, we note that the END in Andromeda appears to have a different orientation depending on what wavelength of light it is observed in (Lockhart et al. 2018). It is possible that mass segregation could explain this, however, a broader range of stellar masses and stellar evolution would have to be included in our model before we could make detailed comparisons with these observations.

Acknowledgements: I am extremely grateful for the support and advice of my amazing advisor, Ann-Marie Madigan. Many thanks as well to Aleksey Generozov, who provided constant encouragement and guidance throughout this project, and to the rest of my research group for helpful discussions. I'd also like to thank Erica Ellingson and Scot Douglass for serving on my defense committee. This work utilized the RMACC Summit supercomputer, which is supported by the National Science Foundation (awards ACI-1532235 and ACI-1532236), the University of Colorado Boulder, and Colorado State University. The Summit supercomputer is a joint effort of the University of Colorado Boulder and Colorado State University.

REFERENCES

Alexander, R. D., Armitage, P. J., Cuadra, J., & Begelman, M. C. 2008, ApJ, 674, 927

Alexander, R. D., Begelman, M. C., & Armitage, P. J. 2007, ApJ, 654, 907

Alexander, T., & Hopman, C. 2009, ApJ, 697, 1861

Amaro-Seoane, P., Audley, H., Babak, S., et al. 2017, arXiv e-prints, arXiv:1702.00786

Arcavi, I., Gal-Yam, A., Sullivan, M., et al. 2014, ApJ, 793, 38

Auchettl, K., Guillochon, J., & Ramirez-Ruiz, E. 2017, ApJ, 838, 149

Bahcall, J. N., & Wolf, R. A. 1977, ApJ, 216, 883

Bartko, H., et al. 2010, ApJ, 708, 834

Chornock, R., Berger, E., Gezari, S., et al. 2014, ApJ, 780, 44

Foote, H. R., Generozov, A., & Madigan, A.-M. 2020, ApJ, 890, 175

French, K. D., Arcavi, I., & Zabludoff, A. 2016, ApJL, 818, L21

Gezari, S., Chornock, R., Rest, A., et al. 2012, Nature, 485, 217

Golightly, E. C. A., Coughlin, E. R., & Nixon, C. J. 2019, ApJ, 872, 163. https://ui.adsabs.harvard.edu/abs/2019ApJ...872..163G

Holoien, T. W.-S., Kochanek, C. S., Prieto, J. L., et al. 2016, MNRAS, 463, 3813

Hopkins, P. F., & Quataert, E. 2010, MNRAS, 407, 1529

Kroupa, P. 2001, MNRAS, 322, 231

Kroupa, P., Weidner, C., Pflamm-Altenburg, J., et al. 2013, The Stellar and Sub-Stellar Initial Mass Function of Simple and Composite Populations, ed. T. D. Oswalt & G. Gilmore, Vol. 5 (Berlin: Springer), 115

Lauer, T. R., Faber, S. M., Groth, E. J., et al. 1993, AJ, 106, 1436. https://ui.adsabs.harvard.edu/abs/1993AJ....106.1436L

Lauer, T. R., Faber, S. M., Gebhardt, K., et al. 2005, AJ, 129, 2138

Levin, Y. 2007, MNRAS, 374, 515

Levin, Y., & Beloborodov, A. M. 2003, ApJL, 590, L33

Lockhart, K. E., Lu, J. R., Peiris, H. V., et al. 2018, ApJ, 854, 121

Lu, J. R., Do, T., Ghez, A. M., et al. 2013, ApJ, 764, 155

Lu, W., Kumar, P., & Narayan, R. 2017, MNRAS, 468, 910

Madigan, A.-M., Halle, A., Moody, M., et al. 2018, ApJ, 853, 141

Magorrian, J., Tremaine, S., Richstone, D., et al. 1998, AJ, 115, 2285

Merritt, D. 2013, Dynamics and Evolution of Galactic Nuclei (Princeton, NJ: Princeton University Press)

Mikhaloff, D. N., & Perets, H. B. 2017, MNRAS, 465, 281. https://ui.adsabs.harvard.edu/abs/2017MNRAS.465..281M

Miller, G. E., & Scalo, J. M. 1979, ApJS, 41, 513

Milosavljević, M., & Loeb, A. 2004, ApJL, 604, L45

Paumard, T., Genzel, R., Martins, F., et al. 2006, ApJ, 643, 1011

Rauch, K. P., & Tremaine, S. 1996, NewA, 1, 149

Rees, M. J. 1988, Nature, 333, 523

Rein, H., & Liu, S. F. 2012, A&A, 537, A128

Rein, H., & Spiegel, D. S. 2015, MNRAS, 446, 1424

Rosswog, S., Ramirez-Ruiz, E., & Hix, W. R. 2009, ApJ, 695, 404

Salpeter, E. E. 1955, ApJ, 121, 161

Spitzer, L. 1987, Dynamical evolution of globular clusters (Princeton, NJ: Princeton University Press)

Stewart, G. R., & Ida, S. 2000, Icarus, 143, 28

Stone, N. C. 2015, The Tidal Disruption of Stars by Supermassive Black Holes (Switzerland: Springer International Publishing)

Stone, N. C., & Metzger, B. D. 2016a, MNRAS, 455, 859

—. 2016b, MNRAS, 455, 859

Tremaine, S. 1995, AJ, 110, 628

van Velzen, S. 2018, ApJ, 852, 72

van Velzen, S., Farrar, G. R., Gezari, S., et al. 2011, ApJ, 741, 73

Wang, J., & Merritt, D. 2004, ApJ, 600, 149

Wernke, H. N., & Madigan, A.-M. 2019, ApJ, 880, 42